Shot noise on chaotic chiral devices

M. S. M. Barros,[1] I. R. A. C. Lucena,[1] A. F. M. R. Silva,[1] A. L. R. Barbosa,[2] and J. G. G. S. Ramos[1]
[1]*Departamento de Física, Universidade Federal da Paraíba, 58297-000 João Pessoa, Paraíba, Brazil*
[2]*Departamento de Física, Universidade Federal Rural de Pernambuco, 52171-900 Recife, Pernambuco, Brazil*

(Received 7 January 2019; published 17 May 2019)

We investigate both the conductance and the shot-noise power of a confined chiral device that engenders subtle embedded backscattering mechanisms. We present analytical results and the correspondent numerical confirmation of the chiral electronic sublattice signal. Examples of quantum dots generating chiral symmetries include graphene sheets and topological insulators. The analytical results are universal and exhibit a robust and peculiar signal for an arbitrary number of open scattering channels. We also demonstrate a tunable mechanism of the valleytronics shot-noise power signal through perpendicular magnetic fields and/or the device symmetry edges. The results also indicate a "Fano factor" associated with the main quantum interference term with a universal value of $1/4$ for a quantum dot with symmetric contacts, regardless of external fields and the number of open channels.

DOI: 10.1103/PhysRevB.99.195131

I. INTRODUCTION

Solid-state physics constitutes one of the main scenarios for the development of new theories [1,2]. Since the pioneer studies of Bragg in 1913, many developments were established, from electromagnetism to quantum mechanics. The consolidation of atomic theory and the possibility of stable long-range arrangement in bulk materials decomposed into microscopically periodic substructures guaranteed the formation of emerging symmetries [3] and the nontrivial properties of matter [4–9].

More recently, with the experimental control of graphene flakes connected to a macroscopic source and drain [10,11], electronic transport gains strong impact at the quantum level. Graphene is a periodic structure of carbon atoms arranged in a hexagonal lattice [12,13]. In the Fermi energy level, its electrons can be described with a linear dispersion relationship leading to an effective physics of massless particles traversing the nanostructure in a "relativistic" way or, in other words, the electronic transport at the Fermi velocity can be seen as massless neutrinos described by the Dirac equation [14]. In this scenario, there is the formation of a spinorial structure which, in the case of graphene, is interpreted as new degrees of freedom associated with the sublattice structure. Other structures with sublattice symmetry include the topological insulators whose electrons also satisfy the Dirac equation generating chirality with both experimental and theoretical relevance [12,15–18]. We henceforth use "chiral devices" or "Dirac devices" to designate two-dimensional graphene sheets without impurities, topological insulators, and all structures with sublattice symmetry.

However, despite great efforts, quantum signals of the chiral degrees of freedom are hardly found in quantum electronic transport [15]. The main reason is that the width increase of the terminals connected to the sample creates more channels that easily eliminate the quantum interference corrections from the conductance [19–21]. In particular, the analytical results known show that the correction is insignificant when compared to the main "Ohmic" term. As the main reason for this incipient contribution, we can indicate the fact that conductance is not an observable one that is significantly affected by backscattering [22–24]. In fact, by the formalism of Landauer, the conductance depends basically on tunneling probabilities [25,26]. A manner to introduce backscattering mechanisms would be to introduce nonideal contacts, which link the ideal terminals to the graphene quantum dot. However, contacts can easily compete with sublattice degrees of freedom, which makes this design little enlightening or improper.

Against this backdrop, we propose a set of possibilities for the direct measurement of the quantum transport effects of chiral (sublattice) symmetry in Dirac devices using the shot-noise power as a prominent observable. The shot-noise power occurs even at the null temperature basically as an effect of the discretization of matter and as the spatial extension of the electron wave function [6,27]. Our idea is based on the fact that the shot-noise power carries the terms of backscattering in Landauer-Büttiker's formulation, even with ideal contacts. In the specific case of a chiral structure, we must remember that there is no mathematical way of describing the entire Bravais lattice with a pair of vectors. This suggests the creation of a base that, in turn, naturally induces the formation of sublattices. The necessity of using a base forms Bragg peaks associated with backscattering; i.e., the shot-noise power must offer strong quantum signals of the chiral structure, as opposed to conductance. Therefore, our study will reveal strongly measurable quantum signals associated to the sublattice symmetry and to the transport of relativistic neutrinos without mass.

The work is organized in the following manner: In Sec. II, the scattering formalism needed for the study of graphene and the expressions of Landauer and Büttiker in terms of S-matrix elements is introduced and developed. In Sec. III, the diagrammatic method for the integration over the unitary group on pure ensembles is introduced and we obtain results

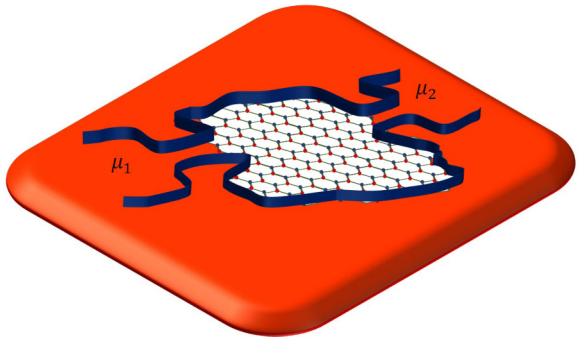

FIG. 1. The quantum dot of graphene connected to two electrochemical potentials through electronic terminals: an example of a chiral or Dirac device. The confinement generates a chaotic effect due to the random edges.

not only for the conductance but also for the shot-noise power, and a numerical simulation is performed to confirm our analytical findings. In Sec. IV, the calculus of crossover between pure ensemble for finite fields is performed. Finally, in Sec. V, the final conclusions are presented.

II. SCATTERING MATRIX FORMALISM

We introduce the scattering model for a chaotic chiral device connected by ideal contacts to two terminals, as shown in Fig. 1. We investigate a quantum dot of graphene large enough to support many resonances coupled to very thin leads, in such a way that a low energy may comprise at least one open channel. In this regime, the mesoscopic fluctuations occur properly in the isospectral (universal) scattering. In graphene flakes, the sublattice symmetry can be broken. The breaking of sublattice symmetry takes place both on the level of the band structure by, e.g., next-nearest-neighbor hopping terms, and by a random potential. Measurement of the band-structure effect indicates a sublattice-symmetry-breaking energy scale of more than 0.1 eV [28]. The electronic universal transport in chiral devices can be described by the scattering matrix

$$\mathcal{S} = \begin{pmatrix} r & t' \\ t & r' \end{pmatrix}, \tag{1}$$

where t (t') and r (r') are transmission and reflection matrix blocks, respectively. Furthermore, the scattering matrix has dimension $2N_T \times 2N_T$, where $N_T = N_1 + N_2$ is the sum of electronic wave propagation modes (channels) (N_i) in each terminal.

Following the Landauer-Büttiker approach [6,29–31], the conductance and the shot-noise power are calculated from the transmission matrix block as

$$G = \frac{2e^2}{h}\mathbf{Tr}(tt^\dagger), \tag{2}$$

and

$$P = \frac{4e^3|V|}{h}\mathbf{Tr}[tt^\dagger(1 - tt^\dagger)]. \tag{3}$$

In the framework of random matrix theory (RMT), the scattering matrix, Eq. (1), associated with the *bipartite lattice* (as two-dimensional square and hexagonal lattices) is classified by chiral class [32], which is divided into three ensembles: the chiral circular orthogonal ensemble $\beta = 1$ (chCOE), which has time-reversal symmetry (TRS), spin-rotation symmetry (SRS), and sublattice/mirror/chiral symmetry (SLS) preserved; the chiral circular unitary ensemble $\beta = 2$ (chCUE), which has TRS broken; and the chiral circular symplectic ensemble $\beta = 4$ (chCSE), which has SRS broken. Furthermore, the scattering matrix can be decomposed as a function of unitary U, and orthogonal and symplectic matrices as in the following [33]:

$$\mathcal{S} = \Sigma_z U^\dagger \Sigma_z U, \quad \Sigma_z \equiv \begin{pmatrix} \mathbf{1_{N_T}} & 0 \\ 0 & -\mathbf{1}_{N_T} \end{pmatrix}. \tag{4}$$

Equation (4) will enable us to use the diagrammatic method developed in Refs. [34,35] to calculate the ensemble averages of Eqs. (2) and (3) in the next sections.

III. UNIVERSAL CONDUCTANCE AND SHOT-NOISE POWER

The transmission matrix blocks are not symmetric, and therefore the ensemble average of Eqs. (2) and (3) is prohibitive. However, through the use of projectors, we can write these equations in terms of the S matrices and, consequently, in terms of the unitary matrices U. This way, it will be possible to develop an integration over the unitary group with the corresponding Haar measure through the diagrammatic method.

A. Mean conductance

We begin with the calculation of the conductance average of the chiral device. Equation (2) can be rewritten as a function of the U-matrix, replacing Eq. (4) within Eq. (2) as in the following:

$$\begin{aligned} g &= \mathbf{Tr}(\mathcal{C}_1 \mathcal{S} \mathcal{C}_2 \mathcal{S}^\dagger) \\ &= \mathbf{Tr}(\mathcal{C}_1 U^\dagger \Sigma_z U \mathcal{C}_2 U^\dagger \Sigma_z U), \end{aligned} \tag{5}$$

where $g = G/(2e^2/h)$ is the dimensionless conductance and the (projectors) matrices C_i are defined as

$$\mathcal{C}_1 = \begin{pmatrix} \mathbf{1_{N_1}} & 0 \\ 0 & 0 \end{pmatrix}, \quad \mathcal{C}_2 = \begin{pmatrix} 0 & 0 \\ 0 & \mathbf{1}_{N_2} \end{pmatrix}, \tag{6}$$

$\mathbf{1}_{N_i}$ being a unity matrix with dimension $N_i \times N_i$.

The ensemble average of Eq. (5) can be calculated by developing the following integral:

$$\langle g \rangle = \int d\mu \mathbf{Tr}(\mathcal{C}_1 U^\dagger \Sigma_z U \mathcal{C}_2 U^\dagger \Sigma_z U), \tag{7}$$

where $d\mu$ is the invariant measure (Haar measure) on a unitary group. One way to calculate the integral is through the diagrammatic method which was developed in Refs. [34,35]. The diagrammatic method is based on the sum of all possible element permutations of the unitary matrix U of the similarity transformations that characterize the chaotic dynamics [36–38].

As we are interested in the chiral device with SLS preserved, we must use the diagrammatic method of Ref. [35] to develop the average over Eq. (5). If the U matrix of Eq. (5) is

unitary, there are four diagrams, while if one is orthogonal or symplectic, there are nine diagrams. The sum of all diagrams gives rise to the following (compact expression) average of conductance:

$$\langle g\rangle = \frac{4\beta N_1 N_2 N_T}{(\beta N_T + 1)(2N_T - 1)}. \tag{8}$$

This result was first obtained in Ref. [35].

A relevant experimental regime happens when the wave propagation number of modes (channels) is large ($N_T \gg 1$). Expanding Eq. (8) in a function of N_T, we have

$$\langle g\rangle = 2\frac{N_1 N_2}{N_T} + \left(1 - \frac{2}{\beta}\right)\frac{N_1 N_2}{N_T^2} + \mathcal{O}\big(N_T^{-1}\big). \tag{9}$$

The first term is the Ohm conductance while the second is known as the localization (main quantum interference correction). The factor 2 in the Ohm term comes from sublattice degenerescence. Furthermore, we take the symmetric terminal case ($N_1 = N_2 = N$) in Eq. (9), and the conductance main quantum interference correction term simplifies to

$$\langle \delta g\rangle = \left(1 - \frac{2}{\beta}\right)\frac{1}{4}. \tag{10}$$

The conductance main quantum interference correction term, Eq. (10), for a chiral device is equivalent to that of the standard quantum dot (QD) described by Wigner-Dyson ensembles [4]. It means that the SLS does not affect the conductance main quantum interference correction in this limit. According to the introduction of the discussion, this fact is due to the absence of backscattering and, consequently, the irrelevance in the semiclassical limit of the double structure of the chiral sublattice. For this reason, it is necessary to study an observable that carries this information even in the semiclassical limit. The shot-noise power, as can be noticed in Eq. (3), contemplates the product of terms of transmission, $tt^\dagger$, and terms of reflection (backscattering), $rr^\dagger = (1 - tt^\dagger)$.

B. Universal shot-noise power

In this section, we investigate in detail how the chiral symmetry affects in a nontrivial way the shot-noise power main quantum interference correction term. Hence, we calculate the average of the shot-noise power, Eq. (3).

First, we rewrite the shot-noise power in a function of a scattering matrix, replacing Eq. (4) within Eq. (3) as follows:

$$\begin{aligned} p &= \mathbf{Tr}(\mathcal{C}_1\mathcal{S}\mathcal{C}_2\mathcal{S}^\dagger) - \mathbf{Tr}[(\mathcal{C}_1\mathcal{S}\mathcal{C}_2\mathcal{S}^\dagger)^2] \\ &= g - \mathbf{Tr}[(\mathcal{C}_1 U^\dagger \Sigma_z U \mathcal{C}_2 U^\dagger \Sigma_z U)^2], \end{aligned} \tag{11}$$

where $p = P/(4e^3|V|/h)$ is the dimensionless shot-noise power and g is the dimensionless conductance which was calculated above in Eq. (8). The average of Eq. (11) can be calculated by developing the following integral:

$$\langle p\rangle = \langle g\rangle - \int d\mu \mathbf{Tr}[(\mathcal{C}_1 U^\dagger \Sigma_z U \mathcal{C}_2 U^\dagger \Sigma_z U)^2], \tag{12}$$

where the last term is composed of eight U matrices.

To develop the integral of Eq. (12), we also use the diagrammatic method [35]. After an extensive algebraic calculation, we identify the 11 024 diagrams that contribute to the average of Eq. (12). The proliferation of diagrams is due to chiral symmetry that doubles the number of unitary matrices in the trace of the shot-noise power whose average is a combinatorial problem. If the U matrix of Eq. (11) is unitary, there are 2 000 diagrams, while if one is orthogonal or symplectic, there are 11 024 diagrams. The sum of these diagrams gives rise to the following average of shot-noise power:

$$\langle p\rangle_{\beta=1} = \frac{4N_1N_2N_T\left[4\left(N_1^2N_2 + N_1N_2^2\right) + 2N_T^2 - 3(N_T - 1)\right]}{(2N_T - 3)(2N_T - 1)(N_T + 3)(N_T + 1)(2N_T + 1)}, \tag{13}$$

$$\langle p\rangle_{\beta=2} = \frac{16N_1N_2N_T(2N_1N_2 - 1)}{(2N_T + 3)(2N_T - 3)(2N_T + 1)(2N_T - 1)}, \tag{14}$$

$$\langle p\rangle_{\beta=4} = \frac{16N_1N_2N_T\left[32\left(N_1^2N_2 + N_1N_2^2\right) - 8N_T^2 - 3(2N_T - 1)\right]}{(4N_T + 3)(4N_T + 1)(2N_T - 3)(2N_T - 1)(4N_T - 1)}, \tag{15}$$

Equations (13)–(15) are the first results of this work. Focusing on the experimental regime limit ($N_T \gg 1$), we expand Eqs. (13)–(15) in a function of N_T, obtaining the following result:

$$\begin{aligned} \langle p\rangle = 2\frac{N_1^2N_2^2}{N_T^3} + \left(\frac{2}{\beta} - 1\right)\frac{N_1N_2(N_1 - N_2)^2}{N_T^4} \\ - \left(\frac{2}{\beta} - 1\right)\frac{N_1^2N_2^2}{N_T^4} + \mathcal{O}(N_T^{-1}). \end{aligned} \tag{16}$$

Notice that the shot-noise power main quantum interference correction obtained from Wigner-Dyson ensembles is only given by the second term of Eq. (16) [4,39]. A central experiment of the full distribution of random values of the shot-noise power and, consequently, of the main quantum interference correction for Wigner-Dyson symmetries (usual semiconductors) was performed in Ref. [40] and further measurements. Hence, we can conclude that the last one is a nontrivial contribution of SLS. We henceforth denominate the exclusive contribution of the graphene as a chiral term (CT), $p_{wl}^{CT} = -(2/\beta - 1)N_1^2N_2^2/N_T^4$. This main quantum interference correction for the shot-noise power is particularly important when the terminals are symmetric (equal number of channels), considering that Schrödinger billiards do not generate interference contributions in this regime.

Taking the symmetric terminal case ($N_1 = N_2 = N$) in Eq. (16), the shot-noise power interference correction simplifies to

$$\langle \delta p\rangle = p_{wl}^{CT} = = \left(1 - \frac{2}{\beta}\right)\frac{1}{16}. \tag{17}$$

Equation (17) shows that the shot-noise power main quantum interference correction term of the chiral device is finite in contrast to one of the standard QD for which the main quantum interference correction term is null in the symmetric configuration [4]. Differently from the conductance main quantum interference correction, Eq. (9), the shot-noise power main quantum interference correction carries information about SLS that could be accessed experimentally.

C. Numerical simulation

In order to confirm Eqs. (13)–(15), we develop a numerical simulation through the Mahaux-Weidenmüller formulation [41]. The scattering matrix of Eq. (4) is written as a function of electronic Fermi energy (ϵ) and the Hamiltonian ($\mathcal{H}$) which describe the resonance states inside the ballistic chaotic quantum dot as follows:

$$\mathcal{S} = \mathbf{1} - 2i\pi\mathcal{W}^{\dagger}(\epsilon - \mathcal{H} + i\pi\mathcal{W}\mathcal{W}^{\dagger})^{-1}\mathcal{W}. \tag{18}$$

The coupling of the resonance states with the propagating modes in the two terminals is carried out by means of the deterministic matrix $\mathcal{W} = (\mathcal{W}_1, \mathcal{W}_2,)$. Moreover, this deterministic matrix does not satisfy direct processes; i.e., the orthogonality condition $\mathcal{W}_i^{\dagger}\mathcal{W}_j = \frac{1}{\pi}\delta_{i,j}$ is maintained to avoid processes whose electrons do not pass through the quantum dot before scattering.

In the framework of RMT, the Dirac Hamiltonian, which describes the graphene, is a member of the Gaussian ensemble (GE) [42]. Furthermore, its entries have the Gaussian distribution given by

$$\mathcal{P}(\mathcal{H}) \propto \exp\left\{-\frac{M}{\lambda^2}\mathrm{Tr}(\mathcal{H}^{\dagger}\mathcal{H})\right\},$$

where $\lambda = M\Delta/\pi$ is the variance related to the electronic single-particle level spacing, Δ, whereas M is the dimension of the $\mathcal{H}$-matrix and number of resonance states supported by the chiral device. To ensure the chaotic regime and consequently the universality of the observables, the number of resonances inside the quantum dot is taken to be large ($M \gg N_T$) [43]. The massless Dirac Hamiltonian satisfies the following anticommutation relation [44]:

$$\mathcal{H} = -\lambda_z\mathcal{H}\lambda_z, \quad \lambda_z = \begin{bmatrix} \mathbf{1}_{2M} & 0 \\ 0 & -\mathbf{1}_{2M} \end{bmatrix},$$

where we interpret the $2M$ of 1's and -1's as the number of atoms in the sublattices A and B of a chaotic graphene quantum dot. The anticommutation relation above implies that the Dirac Hamiltonian is

$$\mathcal{H} = \begin{pmatrix} \mathbf{0} & \mathcal{T} \\ \mathcal{T}^{\dagger} & \mathbf{0} \end{pmatrix}. \tag{19}$$

In the framework of RMT, the massless Dirac Hamiltonian which describes the symmetries of a large chiral device is a member of the chiral Gaussian unitary, orthogonal, or symplectic ensemble [44]. Furthermore, the $\mathcal{T}$-matrix entries have a Gaussian distribution given by

$$P(\mathcal{T}) \propto \exp\left\{-\frac{2M}{\lambda^2}\mathrm{Tr}(\mathcal{T}^{\dagger}\mathcal{T})\right\},$$

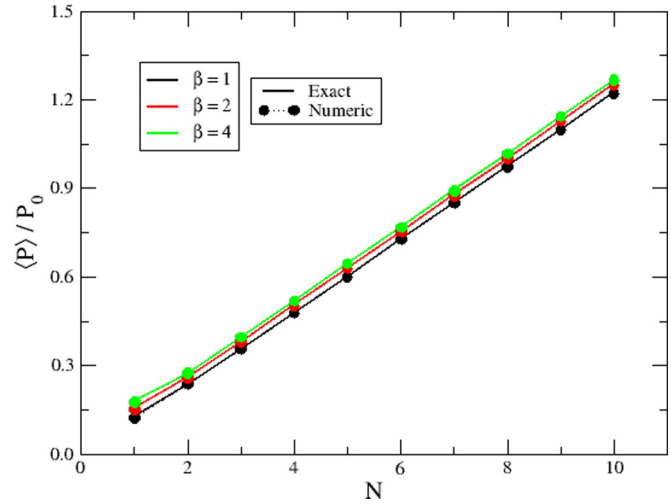

FIG. 2. The ensemble average of the shot-noise power for a quantum graphene dot with symmetric contacts. The symbols are the numerical results data while the lines are the analytical results. Notice a separation between the lines in the three sets of data caused solely by the quantum interference term due to the sublattice symmetry.

where $\lambda = 2M\Delta/\pi$. Using Eqs. (2)–(4), (18), and (19), we developed the numerical simulations for the chiral device that appear in Fig. 2 for full symmetric open channels ($N_i = N$) and in Fig. 3 for asymmetric open channels ($N_1 = 1$ and arbitrary N_2), which was obtained through 2.5×10^4 realizations and with $M = 300$. The circle symbols are the average of the observables whereas the lines represent the analytical results, Eqs. (13)–(15). The numeric simulations are in great accord with the analytical results.

According to Fig. 3, there is a clear distancing between the characteristic curves of each universal symmetry. The immediate implication is the existence of a distinct quantum interference correction for each universal symmetry. However,

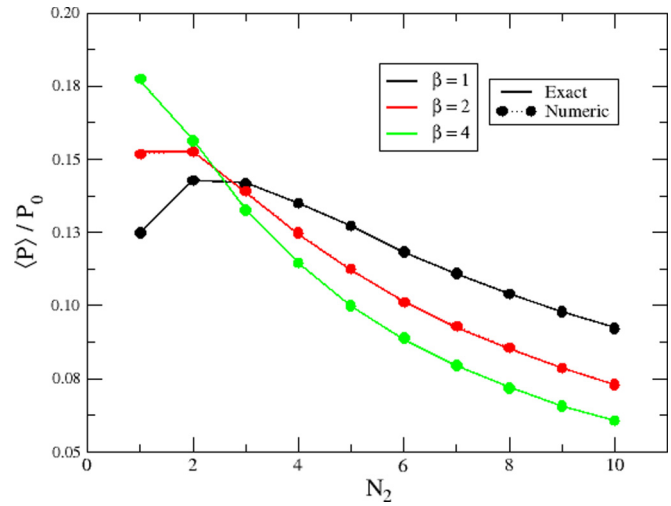

FIG. 3. The ensemble average of the shot-noise power for a quantum graphene dot with asymmetric contacts. The symbols are the numerical results data while the lines are the analytical results. Observe that the curves of the three universal ensembles are separated due to the quantum interference corrections.

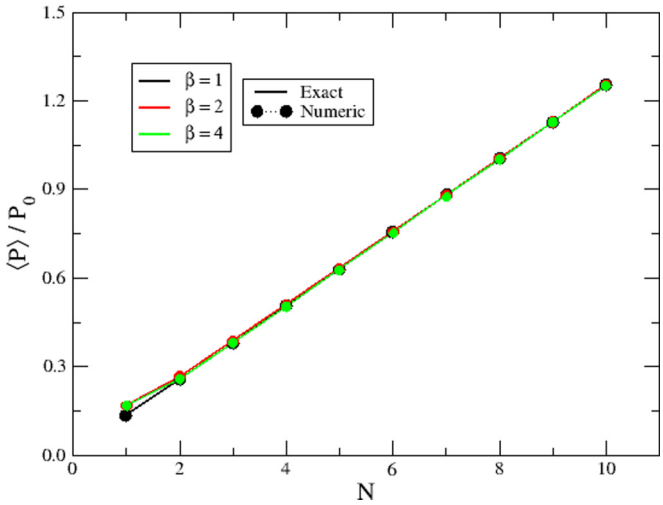

FIG. 4. The ensemble average of the shot-noise power for Schrödinger billiards with symmetric contacts. The symbols are the numerical results data while the lines are the analytical results. Observe that there is no separation between the curves, which characterizes that the quantum interference term disappears when the contacts are symmetrical.

in a more peculiar way, in the curves represented in Fig. 2 the quantum interference in a chiral device gives rise to a separation between the curves even in the symmetric case, a nonexistent feature in the two-dimensional gas of usual semiconductors. This separation is precisely the term p_{wl}^{CT} foreseen in our analytical result. This signal is a fingerprint of an electronic quantum transport in the chiral devices. We executed a simulation of the Wigner-Dyson universal symmetries associated with Schrödinger billiards, i.e., eliminating the Hamiltonian sublattice symmetry. The results for Schrödinger's semiconductors are exhibited in Fig. 4 for full symmetric open channels ($N_i = N$) and Fig. 5 for asymmetric

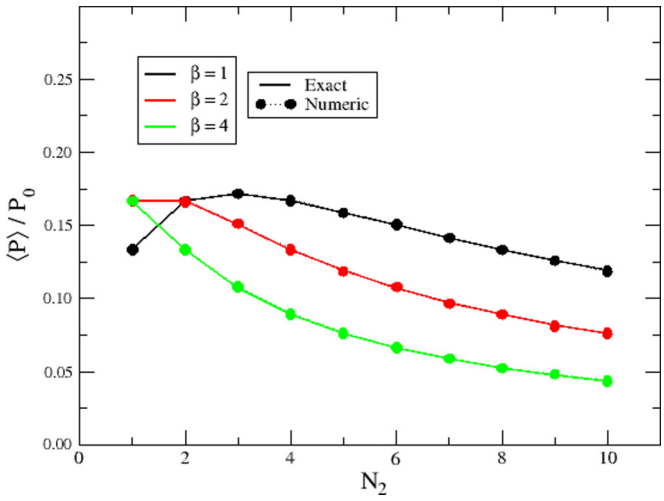

FIG. 5. The ensemble average of the shot-noise power for Schrödinger billiards with asymmetric contacts. The symbols are the numerical results data while the lines are the analytical results. Observe that the curves of the three Wigner-Dyson universal ensembles are separated due to the quantum interference corrections.

open channels ($N_1 = N$ and $N_2 = N_3 = 1$), which was obtained through 2.5×10^4 realizations and with $M = 300$.

IV. CROSSOVER REGIME AND INTERVALLEY SCATTERING

In this section, we investigate how the shot-noise power main quantum interference correction term, Eq. (16), could be affected by external parameters such as magnetic fields, edges, and intervalley scattering of graphene. Therefore, we introduce the stub model [45,46], whose the scattering matrix can be written as

$$\mathcal{S} = \mathcal{P}(1 - \mathcal{Q}^{\dagger}\mathcal{R}\mathcal{Q}\mathcal{U})^{-1}\mathcal{U}\mathcal{P}^{\dagger}, \tag{20}$$

where $\mathcal{P}$ and $\mathcal{Q}$ are projection matrices of dimensions $4N_T\times M$ and $(M-4N_T)\times M$, respectively. The $\mathcal{U}$ matrix is an $M\times M$ random orthogonal matrix taken from chiral ensembles that describes the chiral device. The $\mathcal{R}$ matrix has dimension $(M-4N_T)\times(M-4N_T)$ and is parametrized as [24,47,48]

$$\mathcal{R} = \exp\left[\frac{i}{M}\left(2\pi\frac{\epsilon}{\Delta}\sigma_0\otimes\tau_0 - \mathcal{H}\right)\right]. \tag{21}$$

The $\mathcal{H}$ matrix is obtained from the effective Dirac Hamiltonian preserving its intrinsic symmetries and considering its amplitudes as members of a Gaussian distribution. We consider the additional degrees of freedom residing in the elements of matrices $\mathcal{H}$ which are all proportional to $\sigma_i\otimes\tau_j$, with σ_i and τ_j denoting Pauli matrices ($i, j = x, y, z$) in each subspace of the Dirac Hamiltonian. To perform averages of $\mathcal{S}$, one expands in powers of $\mathcal{U}$ ($M \gg 4N_T$) and uses diagrammatic techniques developed in Ref. [24].

A. Conductance localization main quantum interference correction

Applying Eq. (20) in Eq. (2) and using the diagrammatic method [24], we are able to identify the maximally crossed diagram (Cooperons diagram) that gives rise to the conductance main quantum interference correction,

$$\langle\delta g\rangle = -\frac{N_1N_2}{N_T}\sum_{\rho,\sigma}[\mathbf{Tr}(\mathcal{T}\mathcal{C}\mathcal{T})]_{\rho\sigma;\rho\sigma}, \tag{22}$$

where $\mathcal{T} = \sigma_0\otimes\tau_0\otimes\sigma_y\otimes\tau_0$, and

$$\mathcal{C} = M\sigma_0\otimes\tau_0\otimes\sigma_0\otimes\tau_0 - \mathbf{Tr}(\mathcal{R}\otimes\mathcal{R}^*), \tag{23}$$

where $*$ is the complex conjugation. Equation (22) was first obtained in Ref. [24] by applying the framework to a chiral device subjected to a perpendicular magnetic field and massive boundary.

The valleys correspond to the two inequivalent Fermi points of the graphene band structure [49–51] and constitute relevant implications for the quantum transport, opening applications in the so-called valleytronics. As an application of this method, consider the effective Hamiltonian of a graphene sheet for low energies and long length scales without spin degree freedom given by [22,23,52]

$$H = v[\mathbf{p} - e\mathbf{A}]\cdot\sigma\otimes\tau_0 + u(\mathbf{r})\sigma_0\otimes\tau_0 + u'(\mathbf{r})\sigma_x\otimes\tau_z + w_{ac}(\mathbf{r})\sigma_z\otimes\tau_y + w_{zz}(\mathbf{r})\sigma_z\otimes\tau_z,$$

where the Pauli matrices σ_i and τ_i act on the sublattice and valley degrees of freedom, respectively. The potential vector

$\mathbf{A} = (A_x, 0, 0)$ carries information about the external electromagnetic fields and has no role in coupling the two valleys. The u and u' terms are the long-range impurity potential that induces intervalley scattering; it means that the range of the impurity potential is much larger than the lattice constant [52]. The boundary of the chiral device is described by two physically relevant boundary types, which are known as confinement by the armchair edges term (w_{ac}), and confinement by the zigzag edges term (w_{zz}).

The central property responsible for the simplified random matrix framework in the presence of finite fields is the fact that all relevant time scales are much longer than the electron transit time τ_{erg}; thus, $\tau_B,\ \tau_u,\ \tau_{ac},\ \tau_{zz},\ \tau_{u'} \gg \tau_{erg}$ (the time τ_B is associated with the perpendicular magnetic field and, henceforth, with $\mathbf{A}$). In fact, for a grapheme flake in the transition from classical to quantum regimes, the trajectories can be influenced in distinct ways by the presence of the magnetic field. In the universal regime, however, when many energy levels are available (10^3), all phase space is explored with no preference to some specific trajectories, as long as the dwell time τ_{dwell} is greater than the ergodic time τ_{erg}. In the approach described in the current paper, in the universal regime, $\tau_{dwell} \gg \tau_{erg}$, the results are not affected by special trajectories.

The relevance of the finite fields is guaranteed by the requirement that τ's are of the order of the inverse mean level spacing in the chaotic graphene quantum dot. We may thus introduce the following dimensionless parameters to characterize the intensity of symmetry breaking in the system:

$$x^2 = \frac{2\pi\hbar}{\Delta\tau_B}, \quad u^2 = \frac{2\pi\hbar}{\Delta\tau_u}, \quad u'^2 = \frac{2\pi\hbar}{\Delta\tau_{u'}},$$
$$w_{ac} = \frac{2\pi\hbar}{\Delta\tau_{ac}}, \quad w_{zz} = \frac{2\pi\hbar}{\Delta\tau_{zz}}, \tag{24}$$

where Δ is the mean level spacing.

From the effective Hamiltonian, we can obtain the following expression of the $\mathcal{H}$ matrix [20]:

$$\mathcal{H} = ixX\sigma_x \otimes \tau_0 + iuA_1\sigma_0 \otimes \tau_0 + iu'A_2\sigma_x \otimes \tau_z + iw_{ac}A_3\sigma_z \otimes \tau_y + iw_{zz}A_4\sigma_z \otimes \tau_z.$$

As usual, we assume $\mathcal{H}$ is Hermitian and, consequently, the matrix A_i and X are real antisymmetric and statistically independent with $\langle \mathbf{Tr}(A_iA_j^T)\rangle = \delta_{ij}M^2$ and $\langle \mathbf{Tr}(XX^T)\rangle = M^2$. The parameters x, u, u', and $w_{ac,zz}$ are dimensionless. We replace $\mathcal{H}$ in Eq. (23) and obtain

$$\begin{aligned}\mathcal{C} = {} & \big(N_T + x^2 + u^2 + u'^2 + w_{ac}^2 + w_{zz}^2\big)\sigma_0 \otimes \tau_0 \otimes \sigma_0 \otimes \tau_0 \\ & - x^2\sigma_x \otimes \tau_0 \otimes \sigma_x \otimes \tau_0 \\ & - u'^2\sigma_x \otimes \tau_z \otimes \sigma_x \otimes \tau_z \\ & - w_{ac}^2\sigma_z \otimes \tau_y \otimes \sigma_z \otimes \tau_y \\ & - w_{zz}^2\sigma_z \otimes \tau_z \otimes \sigma_z \otimes \tau_z.\end{aligned} \tag{25}$$

Finally, through substitution of Eq. (25) into Eq. (22), we obtain

$$\begin{aligned}\mathcal{K} &\equiv \sum_{\rho,\sigma} [\mathbf{Tr}(\mathcal{T}\mathcal{C}\mathcal{T})]_{\rho\sigma;\rho\sigma} \\ &= \frac{2}{1+2x^2+2u^2} - \frac{2}{1+2x^2+2u^2+2w_{ac}^2} \\ &\quad + \frac{2}{1+2x^2+2u^2+2u'^2+2w_{zz}^2} \\ &\quad + \frac{2}{1+2x^2+2u^2+2u'^2+2w_{ac}^2+2w_{zz}^2}.\end{aligned} \tag{26}$$

If $u = u' = 0$, we recover the result of Ref. [24]. At this point, considering the zigzag edges, i.e, $w_{zz} \to \infty$, Eq. (26) simplifies to

$$\mathcal{K} = \frac{2}{1+2x^2+2u^2} - \frac{2}{1+2x^2+2u^2+2w_{ac}^2}, \tag{27}$$

which is independent of u'. This indicates that long-range impurities do not induce the intervalley scattering for zigzag nanoribbons as in Ref. [52], which means the quantum interference correction is not affected by intervalley scattering. However, if we take the limit $w_{ac} \to \infty$,

$$\mathcal{K} = \frac{2}{1+2x^2+2u^2} + \frac{2}{1+2x^2+2u^2+2u'^2+2w_{zz}^2}, \tag{28}$$

which is dependent of u'. This means that the intervalley scattering does not vanish even in the case of long-range impurities in the armchair nanoribbons [52], which means the quantum interference correction is affected by intervalley scattering.

B. Shot-noise power main quantum interference correction

We use the RMT/stub framework for the similar calculation of the universal crossover on the shot-noise power. We replace Eq. (20) with Eq. (3). From the 11 024 diagrams used to obtain Eq. (13), we were able to obtain the 45 maximally crossed diagrams (Cooperons diagrams) that contribute to the main quantum interference correction term. After an extensive algebraic calculation we found that the shot-noise power main quantum interference correction is given by

$$\langle \delta p \rangle = \left[\frac{N_1N_2(N_1-N_2)^2}{N_T^3} - \frac{N_1^2N_2^2}{N_T^3}\right]\mathcal{K}. \tag{29}$$

Equation (29) is the second result of this work. Comparing the conductance main quantum interference correction, Eq. (22), and the shot-noise power main quantum interference correction, Eq. (29), we could realize that both are similarly affected by external parameters.

From Eqs. (22) and (29), we can define a universal ("Fano factor") parameter that is unaffected by external perturbation as follows:

$$\frac{\langle \delta p \rangle}{\langle \delta g \rangle} = -\left(\frac{N_1-N_2}{N_1+N_2}\right)^2 + \frac{N_1N_2}{N_T^2}. \tag{30}$$

The ratio between the shot-noise and conductance is generically known as Fano factor. In the same way, this relation between theirs quantum portions defines a parameter first studied in Ref. [39] for a standard QD, whose the result is given by only the first term of Eq. (30). The second one is a contribution of the chiral symmetry in the chiral device. Taking the relevant experimental regime, for which the terminals are symmetrical ($N_1 = N_2$), the first term of Eq. (30) vanishes

while the SLS contribution goes to

$$\frac{\langle \delta p \rangle}{\langle \delta g \rangle} = \frac{1}{4}. \tag{31}$$

The factor $1/4$ is sufficiently large to be accessed experimentally in a chiral device, proving that the chiral symmetry affects in a nontrivial way the shot-noise power main quantum interference correction, which does not happen with the conductance main quantum interference correction.

V. CONCLUSIONS

In this work, we executed a detailed study on the shot-noise power of chiral structures, which has as its main realizations the graphene and topological insulators. The sublattice structure of chiral devices generates additional symmetry that has a strong influence on the backscattering mechanism. We performed an exact analytical calculation in the universal chiral symmetry classes and we showed the emergence of a term that signals the electronic sublattice quantum transport. This term is a fingerprint and can be measured for any number of open channels.

The analytical results were tested through a numerical simulation and were nicely confirmed. We also simulated Schrödinger's billiards and showed that the ensemble average of the shot-noise power coincides in the three ensembles of Wigner-Dyson symmetry (usual semiconductors features) for symmetric contacts. The same does not happen with materials composed of graphene.

Finally, we showed that the Fano factor associated with the main quantum interference correction, which is the reason for the quantum interference correction of the shot-noise power and the conductance interference, generates a universal number $1/4$ for symmetric contacts. The result is robust and does not depend on the "tuning" of graphene edges samples, the applied perpendicular field, or other fields. Despite the dependence (tuning) and even possible suppression of quantum interference regarding such fields, the result $1/4$ occurs in a universal way for all pure ensembles and crossovers between chiral classes. We hope our results contribute for the more general scenario of electronic valley signals. Also, forthcoming investigations in the perspective of sublattice symmetries include chiral ensembles characterized by a topological integer ν, which is the difference of the number of sites on each of the two sublattices [53]. The calculation in the present paper is for $\nu = 0$, but generalizations of the results for $\nu \neq 0$ can indicate several other signals of chirality in mesoscopic devices.

ACKNOWLEDGMENTS

This work was partially supported by Brazilian agencies Conselho Nacional de Desenvolvimento Científico e Tecnológico (CNPq), Coordenação de Aperfeiçoamento de Pessoal de Nível Superior (CAPES), and Fundação de Amparo a Ciência e Tecnologia de Pernambuco (FACEPE).

[1] C. Kittel, *Introduction to Solid State Physics*, 8th ed. (Wiley, New York, 2012).
[2] N. W. Ashcroft and N. D. Mermin, *Solid State Physics* (Harcourt, Orlando, FL, 1976).
[3] P. W. Anderson, Science **177**, 393 (1972).
[4] C. W. J. Beenakker, Rev. Mod. Phys. **69**, 731 (1997).
[5] Y. Alhassid, Rev. Mod. Phys. **72**, 895 (2000).
[6] Ya. M. Blanter and M. Büttiker, Phys. Rep. **336**, 1 (2000).
[7] M. Büttiker, A. Prêtre, and H. Thomas, Phys. Rev. Lett. **70**, 4114 (1993).
[8] Yu. V. Nazarov and Ya. M. Blanter, *Quantum Transport: Introduction to Nanoscience* (Cambridge University Press, Cambridge, UK, 2009).
[9] E. Akkermans and G. Montambaux, *Mesoscopic Physics of Electrons and Photons* (Cambridge University Press, Cambridge, UK, 2007).
[10] K. A. Ritter and J. W. Lyding, Nat. Mater. **8**, 235 (2009).
[11] A. D. Güçlü, P. Potasz, and P. Hawrylak, Phys. Rev. B **84**, 035425 (2011).
[12] A. H. Castro Neto, F. Guinea, N. M. R. Peres, K. S. Novoselov, and A. K. Geim, Rev. Mod. Phys. **81**, 109 (2009).
[13] S. Das Sarma, Shaffique Adam, E. H. Hwang, and E. Rossi, Rev. Mod. Phys. **83**, 407 (2011).
[14] M. O. Goerbig, Rev. Mod. Phys. **83**, 1193 (2011).
[15] J. R. Wallbank, D. Ghazaryan, A. Misra, Y. Cao, J. S. Tu, B. A. Piot, M. Potemski, S. Pezzini, S. Wiedmann, U. Zeitler, T. L. M. Lane, S. V. Morozov, M. T. Greenaway, L. Eaves, A. K. Geim, V. I. Fal'ko, K. S. Novoselov, and A. Mishchenko, Science **353**, 575 (2016).
[16] K. S. Novoselov, A. K. Geim, S. V. Morozov, D. Jiang, M. I. Katsnelson, I. V. Grigorieva, S. V. Dubonos, and A. A. Firsov, Nature (London) **438**, 197 (2005).
[17] Y. Zhang, Y. W. Tan, H. L. Stormer, and P. Kim, Nature (London) **438**, 201 (2005).
[18] M. L. Sadowski, G. Martinez, M. Potemski, C. Berger, and W. A. de Heer, Phys. Rev. Lett. **97**, 266405 (2006).
[19] M. A. Mueed, Md. Shafayat Hossain, I. Jo, L. N. Pfeiffer, K. W. West, K. W. Baldwin, and M. Shayegan, Phys. Rev. Lett. **121**, 036802 (2018).
[20] S. Caneva, P. Gehring, V. M. García-Suárez, A. García-Fuente, D. Stefani, I. J. Olavarria-Contreras, J. Ferrer, C. Dekker, and H. S. van der Zant, Nat. Nanotechnol. **13**, 1126 (2018).
[21] P. Gehring, H. Sadeghi, S. Sangtarash, C. S. Lau, J. Liu, A. Ardavan, J. H. Warner, C. J. Lambert, G. Andrew D. Briggs, and J. A. Mol, Nano Lett. **16**, 4210 (2016).
[22] J. Wurm, K. Richter, and I. Adagideli, Phys. Rev. B **84**, 075468 (2011); J. Wurm, M. Wimmer, and K. Richter, *ibid.* **85**, 245418 (2012).
[23] J. Wurm, A. Rycerz, I. Adagideli, M. Wimmer, K. Richter, and H. U. Baranger, Phys. Rev. Lett. **102**, 056806 (2009).
[24] J. G. G. S. Ramos, M. S. Hussein, and A. L. R. Barbosa, Phys. Rev. B **93**, 125136 (2016).
[25] Pe Yu, Zi-Yuan Li, Hong-Ya Xu, Liang Huang, Barbara Dietz, Celso Grebogi, and Ying-Cheng Lai, Phys. Rev. E **94**, 062214 (2016).
[26] M. Büttiker, Phys. Rev. Lett. **57**, 1761 (1986).
[27] C. W. J. Beenakker and C. Schonenberger, Phys. Today **56**(5), 37 (2003).

[28] A. Kretinin, G. L. Yu, R. Jalil, Y. Cao, F. Withers, A. Mishchenko, M. I. Katsnelson, K. S. Novoselov, A. K. Geim, and F. Guinea, Phys. Rev. B **88**, 165427 (2013).
[29] L. S. Levitov, in *Quantum Noise in Mesoscopic Systems*, edited by Yu. V. Nazarov (Kluwer, Dordrecht, 2003).
[30] Ying-Cheng Lai, Hong-Ya Xu, L. Huang, and C. Grebogi, Chaos **28**, 052101 (2018).
[31] C. H. Lewenkopf, E. R. Mucciolo, and A. H. Castro Neto, Phys. Rev. B **77**, 081410(R) (2008).
[32] P. Jacquod, R. S. Whitney, J. Meair, and M. Büttiker, Phys. Rev. B **86**, 155118 (2012).
[33] S. M. Nishigaki, D. M. Gangardt, and A. Kamenev, J. Phys. A: Math. Gen. **36**, 3137 (2003).
[34] P. W. Brouwer and C. W. J. Beenakker, J. Math. Phys. **37**, 4904 (1996).
[35] M. S. M. Barros, A. J. Nascimento Júnior, A. F. Macedo-Junior, J. G. G. S. Ramos, and A. L. R. Barbosa, Phys. Rev. B **88**, 245133 (2013).
[36] T. Guhr, A. Müller-Groeling, and H. A. Weidenmüller, Phys. Rep. **299**, 189 (1998).
[37] P. Braun, S. Heusler, S. Müller, and F. Haake, J. Phys. A: Math. Gen. **39**, L159 (2006).
[38] I. Hagymási, P. Vancsó, A. Pálinkás, and Z. Osváth, Phys. Rev. B **95**, 075123 (2017).
[39] B. Béri and J. Cserti, Phys. Rev. B **75**, 041308(R) (2007).
[40] S. Gustavsson, R. Leturcq, B. Simovič, R. Schleser, T. Ihn, P. Studerus, K. Ensslin, D. C. Driscoll, and A. C. Gossard, Phys. Rev. Lett. **96**, 076605 (2006).
[41] C. Mahaux and H. A. Weidenmuller, *Shell Model Approach to Nuclear Reactions* (North-Holland, Amsterdam, 1969).
[42] M. L. Mehta, *Random Matrices* (Academic Press, New York, 1991).
[43] J. G. G. S. Ramos, A. L. R. Barbosa, D. Bazeia, M. S. Hussein, and C. H. Lewenkopf, Phys. Rev. B **86**, 235112 (2012).
[44] E. V. Shuryak and J. J. M. Verbaarschot, Nucl. Phys. A **560**, 306 (1993); J. Verbaarschot, Phys. Rev. Lett. **72**, 2531 (1994).
[45] J. G. G. S. Ramos, A. L. R. Barbosa, and A. M. S. Macêdo, Phys. Rev. B **78**, 235305 (2008); J. Phys. A: Math. Gen. **43**, 075101 (2010).
[46] P. W. Brouwer, J. N. H. J. Cremers, and B. I. Halperin, Phys. Rev. B **65**, 081302(R) (2002).
[47] J. G. G. S. Ramos, A. L. R. Barbosa, and A. M. S. Macêdo, Phys. Rev. B **84**, 035453 (2011).
[48] J. G. G. S. Ramos, A. L. R. Barbosa, D. Bazeia, and M. S. Hussein, Phys. Rev. B **85**, 115123 (2012).
[49] D. Culcer, A. L. Saraiva, B. Koiller, X. Hu, and S. Das Sarma, Phys. Rev. Lett. **108**, 126804 (2012).
[50] O. Gunawan, B. Habib, E. P. De Poortere, and M. Shayegan, Phys. Rev. B **74**, 155436 (2006).
[51] K. Behnia, Nat. Nanotechnol. **7**, 488 (2012).
[52] K. Wakabayashi, Y. Takane, M. Yamamoto, and M. Sigrist, New J. Phys. **11**, 095016 (2009).
[53] I. C. Fulga, F. Hassler, A. R. Akhmerov, and C. W. J. Beenakker, Phys. Rev. B **83**, 155429 (2011).